Marine Technology, Vol. 41, No. 4, October 2004, pp. 200–206

Experimental Study on the Influence of Appendages on a Yacht Rolling at Zero Froude Number

Kim Klaka[1] and **Martin Renilson**[2]

Yachts tend to roll uncomfortably while at anchor, causing discomfort to the crew and passengers, generating additional stresses on equipment, and making such operations as embarking and disembarking hazardous activities. Currently, there is a dearth of data regarding roll motions at zero forward speed for hull shapes dominated by large appendages. Hence, an experimental study into the effect of large appendages on roll motion was undertaken. The model test results are presented, showing how changes in appendage geometry alter the roll response.

Introduction

YACHT OWNERS invest considerable resource in acquiring a yacht that is comfortable and safe. One of their aims is to be able to anchor in secluded bays in a relaxed atmosphere. This aim is lost if the vessel starts to roll.

Roll motion is a nuisance for a variety of reasons:

- It causes sea sickness.
- Crew and passengers may fall and hurt themselves.
- Embarking and disembarking become difficult and possibly dangerous.
- Noise is generated through water slap on the hull and motion of inadequately secured objects.
- Some on-board equipment will not perform adequately.
- Yachts moored alongside a jetty or another yacht may suffer damage.

All yachts roll to a greater or lesser extent when subject to waves. When the vessel is on passage and traveling at reasonable speed, the roll motion may be limited through forces generated by the flow around the hull or by the use of fin stabilizers. For sailing yachts, additional roll reduction is obtained from aerodynamic forces. However, when the vessel is moving slowly, or is at anchor, those roll-stabilizing forces are not present.

Currently there is a dearth of data regarding roll motions at zero forward speed for hull shapes dominated by large appendages. Such lack of data means that there are currently no validated numerical prediction methods available to designers of these craft. This makes it very difficult for them to optimize their hull configurations to reduce roll motion. Hence, an experimental study into the effect of large appendages on roll motion was undertaken.

The equation of motion of a yacht rolling may be written in its simplest form as a linear uncoupled equation:

$$(A_{44} + I_{44})\ddot{x}_4 + B_{44}\dot{x}_4 + C_{44}x_4 = M_4 \qquad (1)$$

The solution of equation (1) varies both with wave frequency and amplitude. The roll characteristics of the yacht are described by the equation coefficients. The search for roll minimization requires an understanding of the design factors affecting these coefficients.

The roll mass moment of inertia comprises the structural roll inertia of the yacht and the inertia of the water particles surrounding the yacht that are accelerated as a consequence of the yacht motion—the added inertia. The added inertia of the surrounding water is determined by the underwater shape of the vessel. A yacht with semicircular cross sections and very small appendages will have very little added inertia. A yacht with sections that are more square or triangular in shape will have a higher added inertia, as water must be accelerated as the shape rolls through the water (Vugts 1968). A keel will contribute significantly to added inertia, as some of the water must accelerate with it as it rolls (Newman 1977, Klaka et al 2001).

Roll damping is generated by a number of mechanisms. The biggest contribution often comes from generating vortices as the yacht rolls. Vortices are most easily generated at sharp edges associated with chines, keels, and rudders. The next most significant contribution comes from generating waves as the yacht rolls. A yacht hull with square or triangular sections will generate more waves as it rolls than does a yacht with circular sections. There is also a damping contribution from the friction between the water and the rolling yacht, but this is usually so small it can be neglected.

This paper describes experiments conducted at zero Froude number in a wave basin at the Australian Maritime College using a circular cross section model with different appendages. The aim of the program was to determine the influence on roll motion of:

- Size of appendage
- Foil section of appendage
- Linearity of response with respect to wave amplitude
- Wave heading.

The program also provided validation data for a numerical model written by one of the authors (Klaka et al 2001).

Methodology

The model tests were conducted using a circular cylinder hull. This hull shape was chosen in order to minimize the wave damping and vortex damping from the hull, thus allowing appendage effects to dominate the results. The canoe body draft was similar in characteristic dimensions (length: beam ratio, length:displacement ratio, etc.) to that for a yacht hull. Thus, the tests were able to be conducted with free surface and canoe body influences on the appendages similar to those found on full-scale yachts. The model was free

[1] Centre for Marine Science and Technology, Curtin University of Technology, Perth, Australia.
[2] Centre for Marine Technology, QinetiQ, Gosport, UK.
Manuscript received at SNAME headquarters March 2004.

to roll, pitch, and heave, with the rig attachment points at the waterline to minimize roll moments caused by sway and yaw restraint. Three appendage geometries were chosen for investigation:

- A full-depth rectangular planform flat-plate keel (Fig. 1, top)
- A half-depth rectangular planform flat-plate keel (Fig. 1, bottom) with half the span of the keel shown in Fig. 1, top
- A full-depth rectangular planform aerofoil section keel (Fig. 2).

The roll peak frequency was kept within the range of wave frequencies available in the wave basin. This required the minimization of roll structural mass moment of inertia and maximization of transverse metacentric height (GM_T). The variations in keel configuration used resulted in small mass and buoyancy changes. Because the objective was to measure the hydrodynamic variations between keels and to validate that aspect of the numerical model, the mass of the wave basin model was varied slightly in order to keep the flotation plane and natural roll frequency (in air) constant. The latter was achieved by moving small corrector masses transversely and vertically as required.

The tests were conducted in regular waves at constant wave amplitude rather than constant wave slope. The International Towing Tank Conference (ITTC) recommended procedures for seakeeping model tests allow for either approach (Koterayama 2002). If constant wave slope had been used, the amplitudes at the higher frequencies would have been too small for accurate measurement. The maximum amplitudes used were determined from constraints of deck edge immersion and rig clearance over the model. Wave steepness ranged from 1/294 to 1/46, which compares with the ITTC recommendation of 1/50. The steepness limit for wave breaking in the water depth used is 1/10 (Mehaute 1976).

Free roll decay tests were conducted for comparison with numerical simulation of unforced roll motion.

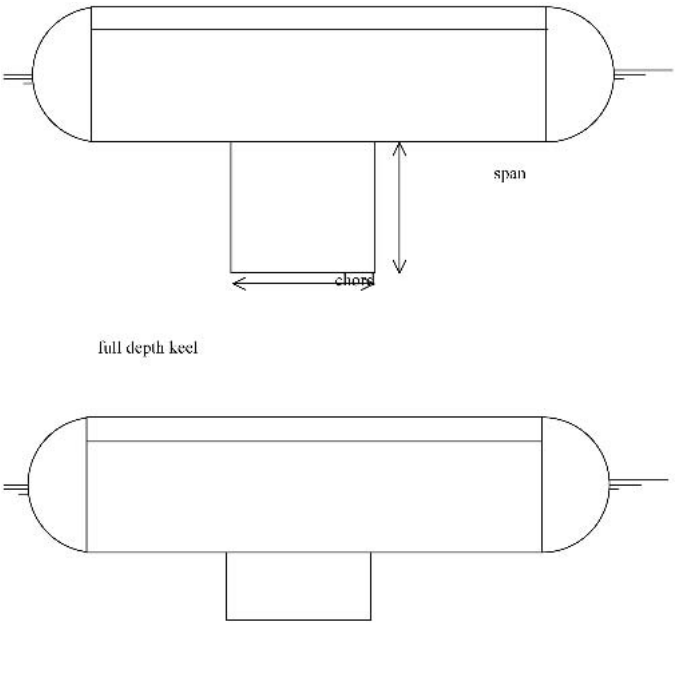

Fig. 1 Keel planforms

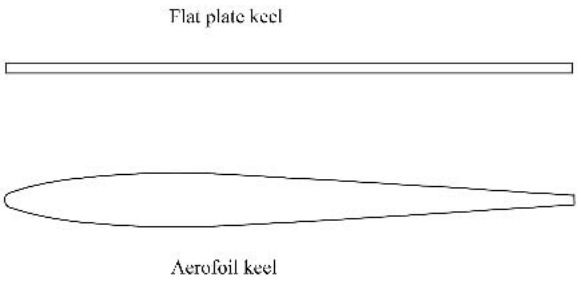

Fig. 2 Keel profiles

Equipment

The model test basin was 35 m long, 12 m wide with water depth set at 0.7 m for these tests. The basin was equipped with a multielement wavemaker, capable of producing regular waves. The wavemaker was controlled from a dedicated PC using proprietary software. A beach was situated at the downstream end of the basin. The basin sides were vertical, and the bottom was flat.

The model was circular cross section, 0.315 m in diameter and 1.3 m long. A hollow foam hemisphere was attached at each end to reduce viscous and free surface end effects. A plywood daggerboard case was installed into which could be slotted one of the three keel configurations. The full- and half-depth keels were made of 6-mm ply, 0.3-m chord, and span 0.3 m and 0.15 m, respectively (Fig. 1). The aerofoil section keel was made by adding a shaped fairing to each face of the full-depth flat-plate keel. The foil was based on a NACA 0010 section with the aft portion thickened to accommodate a 6-mm-wide trailing edge (Fig. 2).

When the keels were changed, they were resealed and the model reballasted to maintain constant flotation waterline

Nomenclature

A_{44} = roll added mass moment of inertia (kg m^2)
B_{44} = roll damping coefficient (N m s)
C_{44} = roll restoring coefficient (N m rad^{-1})
f = wave frequency (Hz)
g = acceleration due to gravity (m s^{-2})
I_{44} = roll structural mass moment of inertia (kg m^2)
GM_T = transverse metacentric height (m)
k = wave number (m^{-1})
M_4 = wave exciting moment (N m)
RAO_{x4} = roll response amplitude operator (dimensionless)
s = span (m)
w = dimensionless frequency (defined in equation [4])
x_4 = roll angle (rad)
$\dot{x}_4 = (dx_4)/(dt)$ = roll velocity (rad s^{-1})
$\ddot{x}_4 = (d_2x_4)/(dt^2)$ = roll acceleration (rad s^{-2})
β_{x4} = linear roll damping coefficient (dimensionless, defined in equation [2])
Δ_m = mass displacement (kg)
ζ_a = wave amplitude (m)
μ = wave heading (rad)
σ_{x4} = standard deviation of roll response (rad)
σ_ζ = standard deviation of free surface elevation (m)

and natural roll period in air. The required ballast modifications were all calculated by spreadsheet, the changes being second- or third-order effects. The spreadsheet calculated values are shown in Table 1. The mass of the attachment posts was included in the model mass; their mass moments in roll were not included because they were connected by ball joints at the waterline (the effective roll pivot point).

The instrumentation for these experiments comprised three linear voltage displacement transducers (LVDTs) and a wave probe. Additional wave probes were used in the preliminary calibration stage. The LVDTs were attached vertically to the model, one each side amidships at the deck edge and one at the forward attachment post on the model centerline. The roll was determined from the difference in readings between the two LVDTs amidships.

The attachment rig for holding the model in the basin comprised two box-frame support tables (Fig. 3). These were placed on the basin floor approximately 3 m apart. Two heavy section alloy beams bridged these tables, with the model attachment system and LVDTs connected to the beams. The uprights of the steel tables therefore penetrated the free surface slightly ahead and behind the model, approximately one boat length cross-stream from the model.

Procedure

Before the model and its attachment rig were placed in the basin, two wave calibration runs were conducted using an array of five wave probes mounted across the basin, located approximately one third of the basin length downstream from the wavemaker—the same distance as the model would later be deployed. The probes were positioned at 1-m spacing, the first probe being 2.5 m from the basin side. On the second run, a sixth probe was mounted near the basin sidewall. This was the probe used to measure surface elevation for subsequent runs. The probes were calibrated statically using the facility's in-house software.

The model was weighed and ballasted to the correct waterline based on the calculated hydrostatics, then launched and checked visually against the marked waterline. Next, the model was installed in the first instance across the basin one third of the basin length downstream of the wavemaker and approximately halfway across the basin. The wave probe used during the model experiments was located 0.5 m from the basin sidewall and 0.035 m downstream of the model. The LVDTs were calibrated statically. The signals from all channels were analogue voltage, acquired digitally at 100 Hz for 30 seconds without filtering or amplification.

On completion of the beam sea tests, the support tables and attachment system were moved so as to align the model 120 deg to the waves (following seas were defined as 0 deg). Runs were also conducted in calm water to measure the free roll decay, and an inclining experiment was carried out to measure the transverse metacentric height GM_T. At the end of the tests the model was reweighed, then mounted on a roll table, and the vertical center of gravity (VCG) was measured.

Table 1 Model variations, calculated by spreadsheet

	Full-Depth Keel	Half-Depth Keel	Aerofoil Keel
Mass (kg)	47.12	46.85	48.42
GM_T (m)	0.0991	0.0998	0.0968
BM_T (m)	0.072	0.073	0.070
M_T below waterline (m)	–0.0041	–0.0063	0.0042
VCG below waterline (m)	0.0950	0.0935	0.101
I_{44} (kg m^2)	0.193	0.193	0.195
Natural roll frequency in air (Hz)	2.50	2.50	2.49

Fig. 3 Model attachment rig

Errors

The VCG determined from three different sources (mass spreadsheet, inclining experiment, and roll table experiment) varied with a standard deviation of 0.0035 m (3.8%).

The standard deviation of the wave probe calibration data was 0.16 mm. This amounts to 1.1% of the median wave standard deviation used.

Differences in the wave amplitude at the six probes were detected. The variations were ±3% about the mean value. Up to half of this may be attributable to the calibration error described above. Time variation of the wave amplitude was also evident. It took the form of amplitude modulation, probably a consequence of the wavemaker stroke varying slightly. The resulting error was 1.4% at 0.5 Hz, and at 0.8 Hz it was 0.5%. The phase angles of the wave probes were found to differ between each other by less than ±3 deg.

The standard deviation of the LVDT static calibration data was 1.7% of the mean roll standard deviation. The error induced by time variation was 1.2% at 0.5 Hz, and at 0.8 Hz it was 0.85%.

The standard deviation of the phase angles was estimated at 10 deg, which amounted to 2.8% of the motion period.

Error bars shown in the figures are for 90% confidence limits assuming a Gaussian distribution of errors.

Results and discussion

Results are shown in Tables 2 to 8.

Free roll decay

Roll decay tests were conducted for two runs, with the full-depth keel fitted. The time series were normalized by dividing by the initial heel angle; the results are shown in Fig. 4. Whereas the natural periods agreed closely, the decay rate differed between the two runs. Analysis of the free decay tests was based on the solution to the linear single degree of freedom roll motion equation (1) with the wave excitation moment set to zero, yielding a linear damping coefficient:

$$\beta_{x4} = \frac{B_{44}}{2\sqrt{([A_{44} + I_{44}]C_{44})}} \tag{2}$$

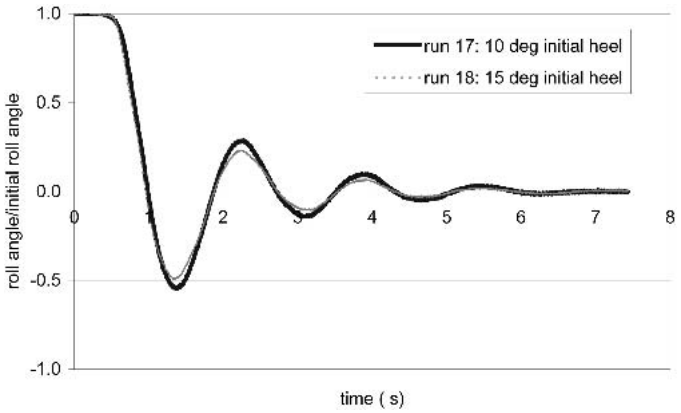

Fig. 4 Normalized roll decay time series, full-depth keel

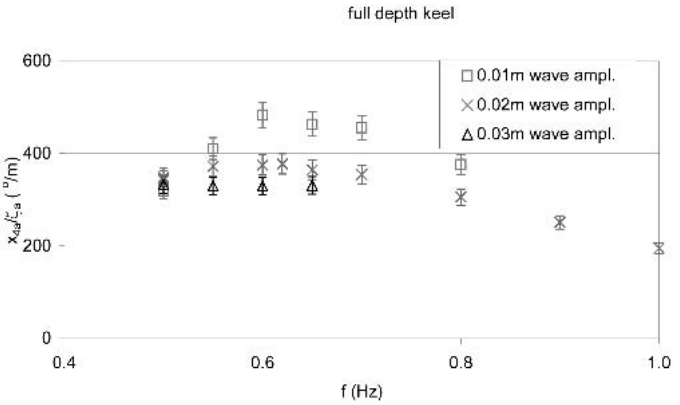

Fig. 5 Effect of wave amplitude on roll response

Note that the factor 2 in equation (2) is omitted in some texts.

The raw data were de-trended, zero-meaned, smoothed with a five-point moving average, then decimated prior to identifying the amplitude peaks, in order to avoid spurious secondary peaks. A third-order polynomial was then fitted to the resulting curve of declining angles, from which the damping coefficient β_{x4} was derived. Mean values are given in Table 2. The relationship between decay rate and damping is complicated for a hull with an appendage, because the appendage damping and inertia are functions of roll acceleration and velocity, respectively, so the roll amplitude, frequency, and decay rate are interdependent.

Data processing for tests in waves

Spatial variation of the wave field was accounted for by calculating an attenuation factor from the standard deviations of the multiprobe runs, to determine the wave surface elevation at the model from the measurements taken at the side probe. The spatial attenuation factor was applied to the wave probe signal, and it was then phase shifted to account for the downstream separation between the probe and the model, using full intermediate-depth linear wave theory. The data set was then reduced to the nearest number of integer cycles, and the standard deviation was calculated. Standard deviations were then used throughout any subsequent processing. Response amplitude operators (RAOs) were calculated using the standard deviations of the free surface elevation and motion response:

$$\mathrm{RAO}_{x4} = \frac{\sigma_{x4}}{k\sigma_{\zeta}} \tag{3}$$

Amplitudes were calculated (for display purposes only) from the standard deviation by assuming that the signal was a single-frequency sinusoid. The motion phases were calculated from the complex transfer function.

Linearity of roll with respect to wave amplitude

Tests were conducted with the full-depth keel in beam seas for three wave amplitudes over a range of frequencies. The results are shown in Fig. 5. The vertical ordinate used is the ratio of roll amplitude to wave amplitude. This shows the degree of linearity with respect to wave amplitude more clearly than if the dimensionless RAO is used, because the RAO is the ratio of roll amplitude to wave slope, not wave amplitude. The results were in accordance with the trends found by other researchers, for example, Robinson and Stoddart (1987) and Spouge (1991), in that the relative response decreased with increasing wave amplitude, indicating nonlinear damping. The effect of wave amplitude on phase angle (Fig. 6) was to decrease the phase angle with increasing wave amplitude at a given frequency.

Table 2 Mean roll decay results

	Period (s)	β_{x4}
Run 17	1.593	0.148
Run 18	1.663	0.149
Mean	1.628	0.1485

Effect of appendages on roll

The influence of appendage configuration on roll response is shown in Fig. 7. The same data are presented in nondimensional form in Fig. 8, using RAO_{x4a} (equation [3]) as the vertical ordinate and dimensionless frequency w for the horizontal ordinate:

$$\mathrm{w} = \omega\sqrt{\frac{s}{g}} \tag{4}$$

The main disadvantage of using a dimensionless plot was the interconnectivity of the two ordinates: the keel span s was used to nondimensionalize the frequency; thus, the results for the two keels with different spans appearing at a given location along the x-axis would be at different wave frequencies. However, the RAO is itself a function of wave frequency (via wave slope), so even if the roll response amplitude for the two keels were the same at that dimensionless frequency w, the RAOs would be different. This was considered to be a misleading way of displaying the data for the

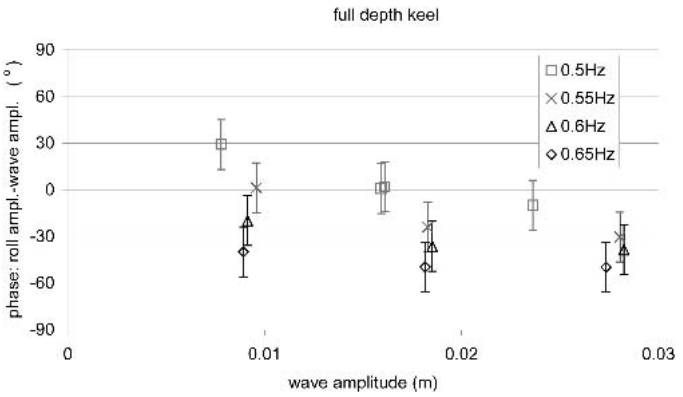

Fig. 6 Effect of wave amplitude on roll phase

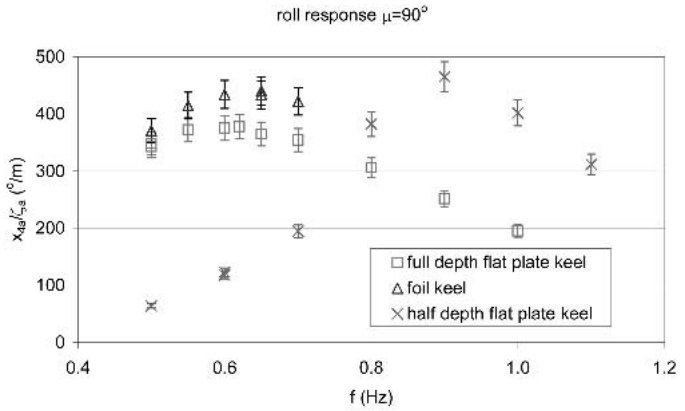

Fig. 7 Effect of appendages on roll amplitude, 0.02 m wave amplitude

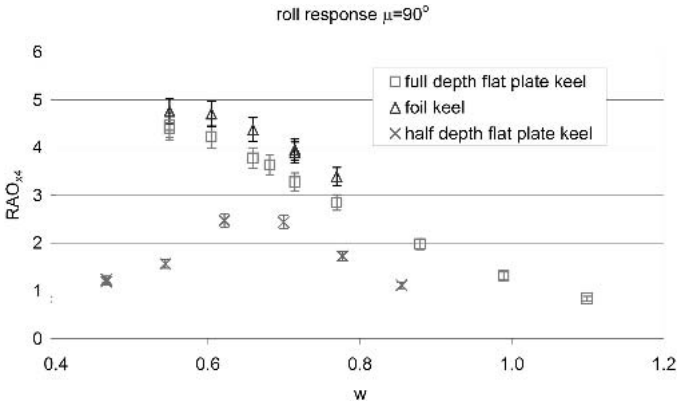

Fig. 8 Effect of appendages on roll amplitude, nondimensional display

purposes of comparing results from different runs. Nevertheless, dimensionless plots were considered valuable for scaling purposes.

The peak frequency from a range of sources is shown in Table 3. The RAO value is from the dimensionless plot (Fig. 8), the amplitude value is from the dimensional plot (Fig. 7), and the phase angle value is from Fig. 9.

The phase angle at resonance for a lightly damped single degree of freedom system is 90 deg between input and output. For a rolling vessel, this corresponds to the phase between the wave slope and the roll angle. Figure 9 shows phase between roll motion and wave amplitude, which is 90 deg lagged from wave slope. Therefore, resonance for a lightly damped single degree of freedom system would occur at a phase angle of 0 deg in this plot.

For the full-depth keel, the frequency of peak response from the dimensionless RAO and the phase plots agreed well. The values for the foil keel followed those of the full-depth keel. The values from the various sources for the half-depth keel were in closer agreement with one another than for the full-depth keel. This was attributed to the reduced damping, possibly leading to reduced nonlinearity.

Table 3 Comparison of peak frequencies (Hz)

Source	Full-Depth Plate Keel	Full-Depth Aerofoil Keel	Half-Depth Plate Keel
RAO plot	0.5	0.5	0.85
Amplitude plot	0.62	0.62	0.9
Phase angle plot	0.5	0.52	0.82

Table 4 Experimental results: full-depth flat-plate keel, 90-deg heading

Frequency (Hz)	Wave Amplitude (m)	Roll Angle (deg)	Phase Angle (deg)
1	0.0168	3.28	−143
0.9	0.0159	3.98	−110
0.8	0.0171	5.24	−89
0.7	0.0172	6.10	−64
0.6	0.0185	6.94	−36
0.5	0.0159	5.46	1
0.65	0.0182	6.62	−50
0.5	0.0161	5.61	2
0.55	0.0183	6.80	−24
0.62	0.0181	6.85	−44
0.8	0.0083	3.12	−90
0.7	0.0082	3.74	−60
0.5	0.0078	2.49	29
0.55	0.0096	3.93	1
0.6	0.0091	4.42	−20
0.65	0.0090	4.13	−40
0.5	0.0236	7.87	−10
0.55	0.0280	9.26	−30
0.65	0.0273	9.04	−50
0.6	0.0282	9.31	−39

Table 5 Full-depth flat-plate keel, 120-deg heading

Frequency (Hz)	Wave Amplitude (m)	Roll Angle (deg)	Phase Angle (deg)
0.5	0.0163	4.68	21
0.6	0.0187	6.33	−17
0.7	0.0171	5.30	−42
0.65	0.0183	5.87	−32
0.55	0.0193	6.00	−4

Table 6 Half-depth flat-plate keel, 90-deg heading

Frequency (Hz)	Wave Amplitude (m)	Roll Angle (deg)	Phase Angle (deg)
0.5	0.0161	1.02	48
0.6	0.0188	2.22	30
0.6	0.0190	2.33	52
0.7	0.0178	3.46	45
0.8	0.0173	6.60	6
1	0.0176	7.08	−59
0.9	0.0169	7.87	−36
1.1	0.0165	5.14	−75

Table 7 Half-depth flat-plate keel, 120-deg heading

Frequency (Hz)	Wave Amplitude (m)	Roll Angle (deg)	Phase Angle (deg)
0.8	0.0167	5.76	17
0.9	0.0162	6.69	−14
1	0.0175	5.33	−41

The difference in peak frequency between the half-depth keel and the full-depth keel is considerable, and was attributed to a very large added inertia change. A consequence of the peak frequency shift was that the half-depth keel exhibited lower response amplitude than the full-depth keel for a given frequency at frequencies below 0.75 Hz. This observation was supported by the output from a numerical model written by one of the authors (Klaka 2001).

The dimensional plot of Fig. 7 shows the peak roll response for the half-depth keel to be approximately 20% higher than

Table 8 Full-depth aerofoil keel, 90-deg heading

Frequency (Hz)	Wave Amplitude (m)	Roll Angle (deg)	Phase Angle (deg)
0.6	0.0188	8.18	−25
0.5	0.0158	5.85	15
0.65	0.0182	8.00	−42
0.7	0.0173	7.31	−56
0.55	0.0185	7.68	−10
0.65	0.0183	7.94	−42

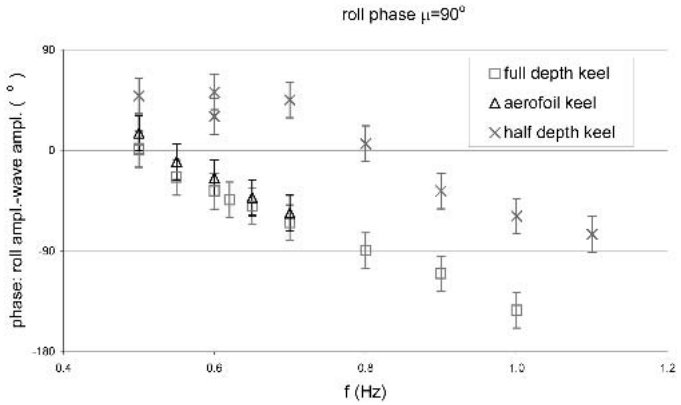

Fig. 9 Effect of appendages on roll phase

for the full-depth keel, albeit at a different wave frequency. This result may be explained by a combination of the following:

- The reduction of edge length reduced the damping (especially the vortex-induced damping) for the half-depth keel, compared with the full-depth keel.
- The change in wave force due to the reduced keel draft.

The nondimensional plot of Fig. 8 shows that the dimensionless response of the half-depth keel is approximately half that of the full-depth keel. This is counterintuitive and is quite probably a consequence of the different peak frequencies. The wave excitation moment at a particular frequency was different for the two keels, owing to the difference in lateral area and span. This makes comparison difficult. If the results are placed in the context of a full-scale yacht rolling at anchor, then for a wave spectrum with amplitude independent of frequency, the full-depth keel will roll less than the half-depth keel. On the other hand, for a wave spectrum with slope independent of frequency, the opposite is true. The wave spectra likely to be experienced by an anchored yacht will lie somewhere between these two conditions.

Figures 7 and 8 show that the response of the aerofoil keel was typically 12% greater than for the flat-plate (full-depth) keel. This may have been a result of reduction in vortex generation round the aerofoil keel due to the rounded edges, particularly the leading edge.

Effect of wave heading on roll

Both the full-depth keel and the half-depth keel were tested at wave headings of 90 deg and 120 deg, at wave amplitude 0.02 m. The results are shown in Figs. 10 to 13. The roll response decreased as wave heading changed from beam seas (90 deg) to oblique seas (120 deg) for both the full-depth keel and the half-depth keel. This outcome was in broad agreement with the trends shown in experiments on other hull forms, such as Schmitke (1978). It was not feasible to

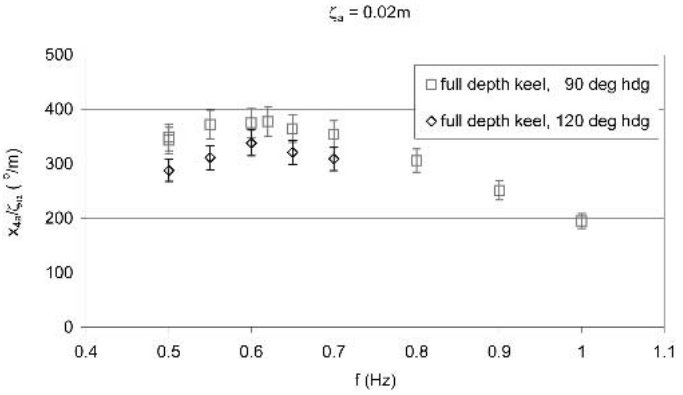

Fig. 10 Effect of wave heading on roll amplitude, full-depth keel

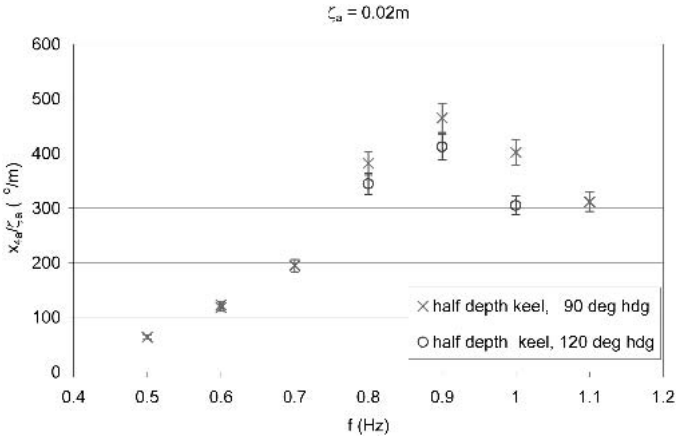

Fig. 11 Effect of wave heading on roll amplitude, half-depth keel

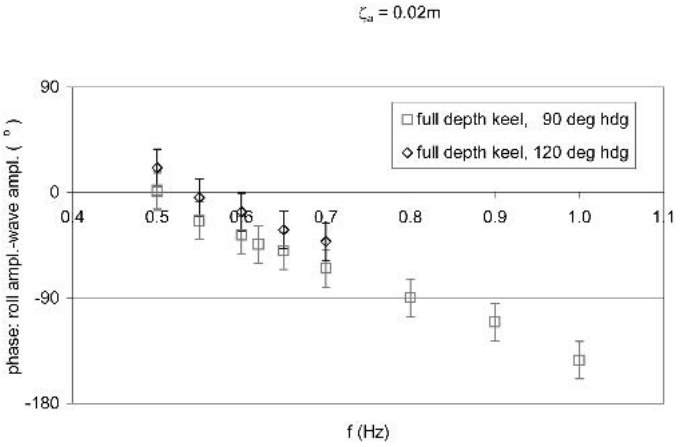

Fig. 12 Effect of wave heading on roll phase, full-depth keel

compare the results quantitatively with those of Schmitke owing to the difference in Froude number and the presentation of his results in stochastic form.

Conclusions

This paper has presented the first comprehensive set of roll motion data for a hull dominated by a large single appendage. It provides the data required to validate numerical models developed to predict the roll motion of such vessels, which are necessary to enable the designers to optimize their design. Specific conclusions follow:

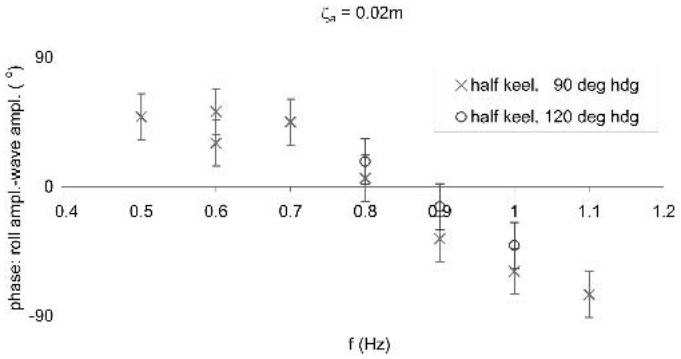

Fig. 13 Effect of wave heading on roll phase, half-depth keel

The roll motion was nonlinear with respect to wave amplitude.

The aerofoil keel exhibited up to 12% greater response than the flat-plate keel, with a similar frequency of peak response. The influence of keel section on roll response merits further investigation.

The half-depth keel exhibited a 50% higher peak response frequency than the full-depth keel. This indicated that the appendage size had a large influence on added inertia. The peak roll amplitude for the half-depth keel was 20% higher than for the full-depth keel. This confirmed that the size of the appendage had a significant influence on damping.

The effect of changing wave heading from beam seas to quartering seas was to reduce the roll response.

Acknowledgments

The authors express their thanks for the technical support provided by Mr. Gregor Macfarlane and his colleagues at the Australian Maritime College.

References

KLAKA, K. 2001 *A Simplified Roll Model*, CMST 2001-09, Centre for Marine Science and Technology, Curtin University of Technology, Perth, 21.

KLAKA, K., KROKSTAD, J., AND RENILSON, M. R. 2001 Prediction of yacht roll motion at zero forward speed, *Proceedings*, 14th Australasian Fluid Mechanics Conference, University of Adelaide, December, Adelaide, Australia.

KOTERAYAMA, W. 2002 *Recommended Procedures: Testing and Extrapolation Methods—Loads and Responses, Sea Keeping, Sea Keeping Experiments*, 7.5-02 07-02.1 International Towing Tank Conference, 16.

MEHAUTE, B. L. 1976 *An Introduction to Hydrodynamics and Water Waves*, Springer-Verlag, New York.

NEWMAN, J. N. 1977 *Marine Hydrodynamics*, MIT Press, Cambridge MA.

ROBINSON, R. W., AND STODDART, A. W. 1987 An engineering assessment of the role on non-linearities in transportation barge roll response, *The Naval Architect*, July/August, 65–79.

SCHMITKE, R. S. 1978 Ship sway, roll and yaw motions in oblique seas, *Transactions of the Society of Naval Architects and Marine Engineers*, **86**, 26–46.

SPOUGE, J. R. 1991 Non-linear roll damping measurements, *Transactions of the Royal Institution of Naval Architects*, **133**, 319–332.

VUGTS, J. H. 1968 *The Hydrodynamic Coefficients for Swaying, Heaving and Rolling Cylinders in a Free Surface,* Technische Hogeschool Delft, report no. 194, 1–56.